High-Resolution NMR Structure and Backbone Dynamics of the Bacillus subtilis Response Regulator, SpoOF: Implications for Phosphorylation and Molecular Recognition † , ‡

ARTICLE *in* BIOCHEMISTRY · SEPTEMBER 1997

Impact Factor: 3.02 · DOI: 10.1021/bi970816l · Source: PubMed

9 AUTHORS, INCLUDING:

James Zapf
Visionary Pharmaceuticals Inc
30 PUBLICATIONS **888** CITATIONS
SEE PROFILE

Frederick W Dahlquist
University of California, Santa Barbara
223 PUBLICATIONS **10,503** CITATIONS
SEE PROFILE

High-Resolution NMR Structure and Backbone Dynamics of the *Bacillus subtilis* Response Regulator, Spo0F: Implications for Phosphorylation and Molecular Recognition[†,‡]

Victoria A. Feher,[§,||] James W. Zapf,[⊥] James A. Hoch,[⊥] John M. Whiteley,[⊥] Lawrence P. McIntosh,[▽] Mark Rance,[@] Nicholas J. Skelton,[#] Frederick W. Dahlquist,*[,§] and John Cavanagh*[,||]

Institute of Molecular Biology and Department of Chemistry, University of Oregon, Eugene, Oregon 97403, Divisions of Cellular Biology and Biochemistry, Department of Molecular and Experimental Medicine, The Scripps Research Institute, 10666 North Torrey Pines Road, La Jolla, California 92037, The Wadsworth Center, New York State Department of Health, Albany, New York 12201, Department of Biochemistry and Molecular Biology, Department of Chemistry and Protein Engineering, Network Centers of Excellence, University of British Columbia, Vancouver, British Columbia, Canada V6T 1Z3, Department of Protein Engineering, Genentech Inc., South San Fransisco, California 94080, and Department of Molecular Genetics, Biochemistry, and Microbiology, University of Cincinnati College of Medicine, 231 Bethesda Avenue, Cincinnati, Ohio 45267

Received April 8, 1997; Revised Manuscript Received June 10, 1997[⊗]

ABSTRACT: NMR has been employed for structural and dynamic studies of the bacterial response regulator, Spo0F. This 124-residue protein is an essential component of the sporulation phosphorelay signal transduction pathway in *Bacillus subtilis*. Three-dimensional ^{1}H, ^{15}N, and ^{13}C experiments have been used to obtain full side chain assignments and the 1511 distance, 121 dihedral angle, and 80 hydrogen bonding restraints required for generating a family of structures (14 restraints per residue). The structures give a well-defined $(\alpha/\beta)_5$ fold for residues 4−120 with average rms deviations of 0.59 Å for backbone heavy atoms and 1.02 Å for all heavy atoms. Analyses of backbone ^{15}N relaxation measurements demonstrate relative rigidity in most regions of regular secondary structure with a generalized order parameter (S^2) of 0.9 ± 0.05 and a rotational correlation time (τ_m) of 7.0 ± 0.5 ns. Loop regions near the site of phosphorylation have higher than average rms deviation values and T_1/T_2 ratios suggesting significant internal motion or chemical exchange at these sites. Additionally, multiple conformers are observed for the $\beta4-\alpha4$ loop and β-strand 5 region. These conformers may be related to structural changes associated with phosphorylation and also indicative of the propensity this recognition surface has for differential protein interactions. Comparison of Spo0F structural features to those of other response regulators reveals subtle differences in the orientations of secondary structure in the putative recognition surfaces and the relative charge distribution of residues surrounding the site of phosphorylation. These may be important in providing specificity for protein−protein interactions and for determining the lifetimes of the phosphorylated state.

Bacillus subtilis responds to nutrient deprivation and high cell density by expressing a group of gene products that transform the bacterium from a vegetative cell to a dormant spore (Hoch, 1993). A signal transduction pathway involving several kinases (KinA and KinB), response regulators (Spo0F and Spo0A), phosphatases (RapA, RapB, and Spo0E), and a phosphotransferase (Spo0B) are responsible for integrating signals regarding the external cell density, metabolic nutrient levels, and the stage of the cell cycle so that sporulation genes are activated only when environmental conditions warrant the lifestyle transition to the endospore form (Burbulys et al., 1991; Perego et al., 1994). Spo0F plays a central role in the integration of these signals (Perego & Hoch, 1996). Spo0F can be phosphorylated by two different kinases (Perego et al., 1989; Trach & Hoch, 1993) and can be dephosphorylated by two different phosphatases (Perego et al., 1994). Activation of these phosphatases either attenuates or short-circuits the signal to initiate sporulation.

Spo0F belongs to a large class of proteins, the response regulators, that participate in many different bacterial signal transduction pathways (Stock, J. B., et al., 1989; Parkinson & Kofoid, 1992). Response regulators contain a domain of ∼120 residues that becomes phosphorylated at one of a triad of conserved aspartate residues in a magnesium-dependent reaction with a histidine autokinase. The formation of the acyl phosphate at the carboxylate of an aspartate residue (Asp54 in Spo0F) activates the protein. Although the three conserved active site aspartate residues (by homology Asp10, Asp11, and Asp54 in Spo0F) of response regulators have been shown to be essential for phosphorylation and activation

[†] The research in this report was supported by NIH Grants GM07759 (V.A.F.), GM33677 (F.W.D.), GM45727 (J.M.W.), and GM19416 (J.A.H.), NSF Grant MCB9221280 (M.R.), and the Canadian Protein Engineering Network Centers of Excellence (L.P.M.).

[‡] The atomic coordinates have been deposited in the Brookhaven Protein Data Bank (1FSP for the ensemble and 2FSP for the minimized mean structure).

* To whom all correspondence should be addressed. J.C. Telephone: (518) 474-6396. Fax: (518) 473-2900. E-mail: johnc@wadsworth.org. F.W.D. Telephone: (541) 346-4036. Fax: (541) 346-5891. E-mail: fwd@nmr.uoregon.edu.

[§] University of Oregon.

[||] New York State Department of Health.

[⊥] The Scripps Research Institute.

[▽] University of British Columbia.

[@] University of Cincinnati College of Medicine.

[#] Genentech Inc.

[⊗] Abstract published in *Advance ACS Abstracts,* August 1, 1997.

S0006-2960(97)00816-7 CCC: $14.00

(Saunders et al., 1989; Bourret et al., 1990), little is known of the role these residues and other highly conserved active site residues (Thr82 and Lys104) play in either of these processes. For some of the response regulators, phosphorylation appears to activate the protein through a conformational change (Stock et al., 1995; Lowry et al., 1994). Structural studies of phosphorylated CheY show conformational changes that propagate away from the site of modification (Lowry et al., 1994). Spo0F, when phosphorylated, binds and transfers its phosphoryl group to Spo0B (Burbulys et al., 1991). Thus, the signal transmitted from activated Spo0F is mediated by transfer of the phosphate rather than exclusively through a conformational response.

The NMR solution structure and backbone dynamics of the apo form of Spo0F are reported here. Analyses of the structure and dynamics give insights into features that influence the site of phosphorylation, namely its characteristic magnesium affinity and relatively long phosphorylated lifetime relative to that of other response regulators. Structural comparisons of Spo0F with response regulators from other signaling pathways indicate general similarities in the molecular architecture utilized by these proteins. However, differences are observed in some regions, suggesting that their involvement in protein−protein interactions is specific to the Spo0F signaling pathway. These surfaces may be important in defining the specificity of sites for protein−protein interactions. Analysis of backbone dynamics reveals regions of Spo0F with a propensity for multiple conformations that interestingly overlap with those identified as potential sites for protein−protein interactions.

EXPERIMENTAL PROCEDURES

Sample Preparation. Uniformly ^{15}N- and ^{15}N-, ^{13}C-labeled SpoOF samples were expressed in *Escherichia coli* BL21DE3 cells and purified as previously described by Zapf et al. (1996). A 10% nonrandomly fractionally ^{13}C-labeled sample was prepared using techniques described by Neri et al. (1989) and Senn et al. (1989). A specifically [$\delta_{1,2}$,$\epsilon_{1,2}$,ζ-^{2}H$_5$]Phe-labeled Spo0F was prepared using a *pheA* auxotrophic DL39 strain and media conditions as described by Muchmore et al. (1989). A [$\delta_{1,2}$,$\epsilon_{1,2}$-^{2}H$_4$]Tyr, uniformly ^{15}N-labeled Spo0F sample was prepared by growing the BL21DE3 strain in minimal media enriched with 300 mg/L [$\delta_{1,2}$,$\epsilon_{1,2}$-^{2}H$_4$]Tyr (Cambridge Isotopes). All NMR samples were 1.0−2.1 mM in protein concentration in 10 mM potassium phosphate, 50 mM KCl, 0.02% NaN_3, and 10% D_2O at pH 6.8−6.9 unless otherwise stated.

NMR Experiments. The following spectrometers were used for data collection: Bruker AMX 600, Bruker DMX 500, Varian Unity 500 equipped with gradient hardware, and GE GN500. Unless otherwise indicated, data were collected using the TPPI−STATES[1] procedure for frequency discrimination in indirect dimensions (Marion et al., 1989a) and GARP decoupling sequences during acquisition (Shaka et al., 1985). Spectra were processed using Felix software (MSI Technologies). In general, spectra were first treated by convolution-based solvent reduction (Marion et al., 1989b), followed by cosine apodization, and zero filled once. Data collected with a constant time for indirect dimensions were processed with mirror image linear prediction (Zhu & Bax, 1992). Spectral referencing is identical to that described in Feher et al. (1995).

Assignments. Side chain carbon assignments were determined from a combination of a sensitivity-enhanced C(CO)-NH (Grzesiek et al., 1993a), HCCH-TOCSY (Bax et al., 1990a), and HCCH-COSY experiments (Bax et al., 1990b; Ikura et al., 1991a) and are reported in the Supporting Information. The HCCH-TOCSY and HCCH-COSY spectra were collected on a sample prepared in 99% D_2O. A 22 ms DIPSI-2 isotropic mixing sequence (Shaka et al., 1988) was used for the HCCH-TOCSY. Carbon chemical shifts were first linked to a previously assigned amide resonance in the C(CO)NH experiment, and then their assignment to a particular atom type was made by comparison to characteristic carbon chemical shifts (Wishart et al., 1991) or by assignment of HCCH-TOCSY and HCCH-COSY resonances as described by Ikura et al. (1991b). In addition, many isoleucine γ-methyl resonances not observed in the C(CO)-NH experiment were assigned using the HCCH-TOCSY spectra. Side chain proton assignments derived initially from a ^{15}N TOCSY-HSQC spectrum (Feher et al., 1995) were confirmed by this procedure. The remaining side chain proton resonance chemical shifts were determined from the H(CCO)NH experiment (Grzesiek et al., 1993a). ^{1}H chemical shift values were correlated with their respective bonded ^{13}C value through the use of HCCH-TOCSY and HCCH-COSY spectra. These spectra were also useful for assignments in long spin systems and prolines.

Aromatic ring carbon and proton assignments were obtained from a combination of the [(Hβ)CβCγCδ]Hδ, (Hβ)Cβ(CγCδCϵ)Hϵ (Yamazaki et al., 1993), and CT-HSQC experiments (Bax et al., 1990b; Norwood et al., 1990). Phenylalanine ζ-protons were assigned from a two-dimensional DQF-COSY spectrum (Rance et al., 1983) collected on a [$\delta_{1,2}$,$\epsilon_{1,2}$-^{2}H$_4$]Tyr, ^{15}N-labeled sample. $^{15}N^{\delta 1}$ and $^{15}N^{\epsilon 2}$ assignments for histidine 101 were determined from an HMBC spectrum (Bax & Summers, 1986) recorded with a single 22 ms delay to generate long range ^{1}H−^{15}N correlations.

Distance Restraints. NOE assignments (531) were determined from previous secondary structure analysis of a three-dimensional ^{15}N NOESY-HSQC spectrum (Feher et al., 1995). Most long range NOEs in this data set were limited to the β-sheet region, with a few NOEs linking the α-helices and β-sheet. The majority of the distance restraints required for the tertiary structure calculations were derived from assignment of NOEs in a three-dimensional simultaneous ^{13}C, ^{15}N-NOESY-HSQC spectrum (Pascal et al., 1994) recorded using a 120 ms mixing time. A three-dimensional ^{13}C-NOESY-HSQC spectrum (Ikura et al., 1991b) was also collected for the same doubly labeled sample in 99% D_2O with a 100 ms mixing time. This latter spectrum was used for assignment and volume integration of cross-peaks involving protons that resonate within 0.8 ppm of the water signal. Severe spectral overlap of the tyrosine and phenylalanine ring protons made analysis of NOEs to these protons difficult and prompted the preparation of the [$\delta_{1,2}$,$\epsilon_{1,2}$,ζ-^{2}H$_5$]Phe and [$\delta_{1,2}$,$\epsilon_{1,2}$-^{2}H$_4$]Tyr specifically labeled samples. Two-dimen-

[1] Abbreviations: COSY, correlation spectroscopy; DQF-COSY, double-quantum-filtered correlation spectroscopy; TOCSY, total correlation spectroscopy; HSQC, heteronuclear single-quantum correlation; CT-HSQC, constant-time HSQC; HMBC, heteronuclear multiple-bond-correlation; NOE, nuclear Overhauser effect; TPPI, time-proportional phase incrementation; rmsd, root mean squared deviation; SA, simulated annealing; pH*, observed pH reading with correction for the isotope effect.

sional NOESY spectra (Jeener et al., 1979) collected on these samples in D_2O were simplified by the absence of four sets of ring protons in each case. NOESY mixing times were 120 ms for the [$\delta_{1,2}$,$\epsilon_{1,2}$,ζ-$^2H_5$]Phe sample and 100 ms for the [$\delta_{1,2}$,$\epsilon_{1,2}$-$^2H_4$]Tyr sample. Distance restraint upper bounds were derived by converting integrated peak volumes for assigned NOE cross-peaks to distance categories in a method similar to that described by Skelton et al. (1995). Initially, distance categories were limited to upper bounds of 3.0, 4.0, and 5.0 Å for strong, medium, and weak NOEs, respectively. During the final stages of the calculations, an additional upper bound limit was added for very strong NOEs of 2.7 Å. All lower bounds were set to van der Waals radii, 1.8 Å. Upper bound limits were adjusted to the weakest category for NOE cross-peaks with overlap (Skelton et al., 1995). Cross-peak volumes derived from methyl groups, degenerate methylene protons, or ring protons were divided by the number of contributing protons prior to categorization (Yip, 1990).

Stereospecific Assignments and Dihedral Angle Restraints. ϕ angle restraints were obtained from the previously reported $^3J_{HN\alpha}$ coupling constants (Feher et al., 1995). These were restrained to $-65 \pm 25°$ for those with a $^3J_{HN\alpha}$ of <6.0 Hz and $-120 \pm 30°$ for amides with a $^3J_{HN\alpha}$ of >8.0 Hz. ϕ angles were restrained to $-89 \pm 90°$ if $^3J_{HN\alpha}$ values were intermediate by analysis of HMQC-J (Feher et al., 1995) or the $HN_i-C^\alpha H_{i-1}$ NOE intensity was greater than the intraresidue $HN_i-C^\alpha H_i$ NOE intensity. Analysis of high-resolution two-dimensional CT ^{13}C-HSQC spectra (Santoro & King, 1992; Vuister & Bax, 1992) of a 3.8 mM nonrandomly 10% fractionally ^{13}C-labeled Spo0F sample collected with the STATES procedure (States et al., 1982) and MLEV16 decoupling during acquisition (Levitt et al., 1982) provided stereospecific assignments for leucine and valine methyl groups (Neri et al., 1989; Senn et al., 1989) as reported in the Supporting Information. Two-dimensional spin echo difference CT HSQC experiments (Vuister et al., 1993; Grzesiek et al., 1993b) were utilized for measuring quantitatively three-bond $^{13}C-^{15}N$ and $^{13}C-^{13}C$ J couplings. The combined knowledge of stereospecific methyl assignments and coupling constants provided χ_1 angle assignments for valine, isoleucine, and threonine side chains according to a staggered rotamer model. Stereospecific assignments for residues with nondegenerate β-methylene protons were derived from analysis of the three-dimensional ^{13}C-NOESY-HSQC and three-dimensional ^{15}N-NOESY-HSQC experiments according to methods described by Wagner et al. (1987). Their χ_1 angles were restrained to -60, 180, or 60 $\pm$ 20° from analysis of a three-dimensional HNHB spectrum (Archer et al., 1991) and a 38 ms three-dimensional ^{15}N-TOCSY-HSQC spectrum (Driscoll et al., 1988) using the staggered rotamer model.

Structure Calculations. Structure calculations were carried out using the program XPLOR version 3.1 (Brünger, 1992). The sub-embedding protocol employing distance geometry was used to generate sets of 60 structures. These structures were refined using the simulated annealing and refinement protocols described by Brünger (1992). Force constants were 50 kcal mol^{-1} Å^{-2} for distance restraints and 200 kcal mol^{-1} rad^{-2} for angle restraints. Several averaging classifications were used depending on the distance restraint type (Nilges, 1993), namely $\langle 1/r^6 \rangle^{1/6}$ averaging for distances between pseudoatoms and center averaging for atoms involving stereospecifically assigned or achiral hydrogens. Initial

Table 1: Summary of Input Restraints Used for Structure Calculations

$^1H-^1H$ distance restraints	
total	1511
intraresidue	518
sequential	296
medium ($1 < \|i-j\| > 5$)	319
long range ($\|i-j\| > 5$)	378
dihedral angle restraints	
φ, χ_1	88, 33
stereospecific assignments	
$C^\beta H_2$, $CH(C^{\gamma,\delta}H_3)_2$	33
hydrogen bond	
β-sheet	26
α-helix	54
total number of restraints/residue	14

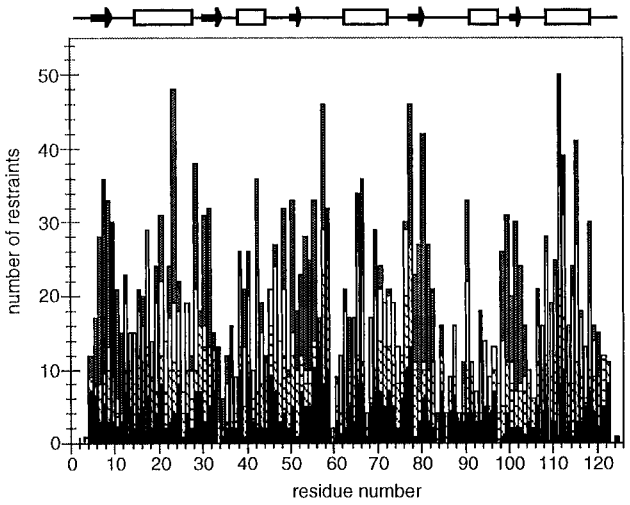

FIGURE 1: Distribution of distance restraints for the Spo0F sequence. The number of intraresidue (black solid), sequential (black diagonals), medium range (empty), and long range (gray shaded) distance restraints for each residue are indicated.

structures were calculated using the preliminary set of 531 NOE-derived distance restraints, 31 ϕ angle restraints, and 82 distance restraints for 41 hydrogen bonds (derived from hydrogen exchange data). Planar geometry restraints for peptide bonds were included ($180 \pm 10°$) for all residues except Lys104-Pro105. A high-field $^{13}C^\gamma$ chemical shift for Pro105 (Richarz & Wüthrich, 1978; Ikura et al., 1991b) suggests that Lys104-Pro105 has a cis peptide bond which was explicitly included in the topology file (Brünger, 1992). Distance restraints were added iteratively through rounds of NOE assignments based on preliminary structures [visualized using the program MIDAS (University of California at San Francisco Computer Graphics Laboratory; Ferrin et al., 1988)] and corrections for distance and angle violations. Stereospecific assignments for 4 valines, 8 leucines, and 17 residues containing nondegenerate β-methylene protons and χ_1 angles for 33 residues were also included. Once there were more than an average of 10 restraints/residue and the backbone rms deviation was ~1.5 Å, an additional distance restraint category of 1.8−2.8 Å was included for large NOE volumes. Additional hydrogen bonding restraints were also added in secondary structure regions. The set of distance and dihedral angle restraints used for calculation of the final structures are summarized in Table 1. Figure 1 illustrates the number of distance restraints used for each residue.

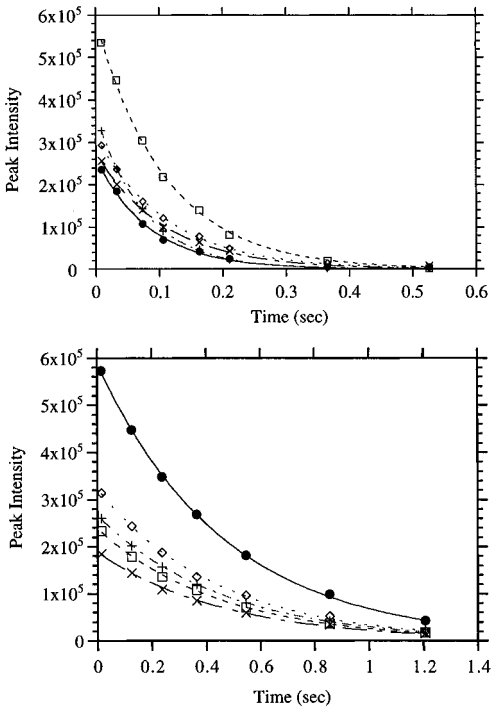

FIGURE 2: ^{15}N T_2 and T_1 relaxation curves. T_2 decay curves (top panel) for residues Leu18 (+), Gln32 (×), Asp49 (◇), Ile63 (□), and Phe102 (●) and T_1 decay curves (bottom panel) for Lys5 (□), Leu53 (+), Lys70 (●), Ala83 (×), and Lys94 (◇).

^{15}N Backbone Relaxation Measurements. ^{15}N relaxation parameters, T_1 and T_2 relaxation rate constants and steady state heteronuclear NOEs, were obtained using experiments described by Barbato et al. (1992). T_1 experiments were collected with delay times of 14, 126, 238, 364, 546, 855 ms and 1.2 s with duplicates of the 14 and 364 ms time points and a relaxation delay of 1.8 s (4 times the average T_1 value). The T_2 measurements were collected at 8, 32, 73, 105, 162, 210, 364, and 525 ms delay times using 8 and 105 ms as duplicates. Analyses of T_1, T_2, and NOE data were carried out according to methods described by Stone et al. (1992) with computer programs generously provided by M. Akke and A. Palmer (Columbia University, New York). Figure 2 illustrates typical fits of data to exponential decay curves for T_1 and T_2 measurements. Figure 3 illustrates the T_1, T_2, and T_1/T_2 values determined for each residue (also see Table 2 in the Supporting Information). Order parameters were calculated according to methods outlined by Kay et al. (1989) using a FORTRAN program described by Zhou et al. (1996). Eighty-eight of the 124 amide nitrogens could be analyzed using this protocol. Of the remaining amides, the first three residues could not be observed, and Ile57, Lys67, Met69, Lys116, and Tyr118 were omitted because of spectral overlap. Several amides could not be fitted to the model described by Kay et al. (1989): Asp11−Gly27, Gly59, Lys70, Thr82, Gly85, Lys94, Thr100, and Phe102.

Structural Comparisons to Other Response Regulators. The coordinates to response regulators *E. coli* CheY (Volz & Matsumura, 1991), *Saccharomyces typhimurium* NtrC (Volkman et al., 1995), and *E. coli* NarL (Baikalov et al., 1996) were obtained from the Brookhaven National Laboratories data base (file names 3CHY, 1NTR, and 1RNL, respectively). The coordinates for the Spo0F Tyr13Ser mutant were kindly given to us by K. Varughese (University

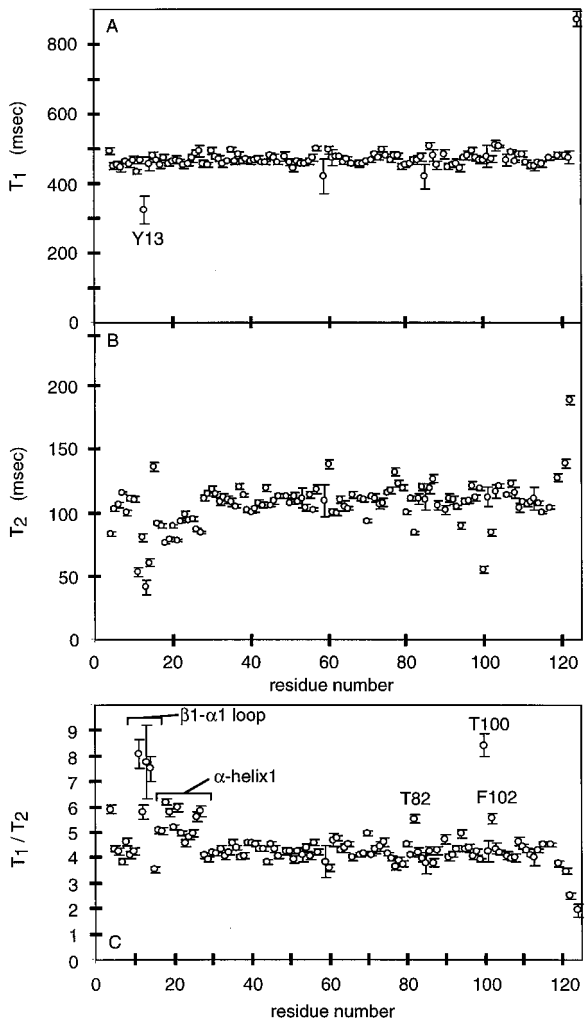

FIGURE 3: ^{15}N T_1, T_2, and T_1/T_2 ratios and uncertainties. Measured T_2 (A), T_1 (B), and derived T_1/T_2 ratios (C) are plotted for each residue number.

of California at San Diego). Although several structures of CheY have been published (Moy et al., 1994; Volz & Matsumura, 1991; Stock, A. M., et al., 1989; Bellsolell et al., 1994), the *E. coli* crystal structure, 3CHY, was chosen for comparisons because it was determined under conditions most similar to those of Spo0F, in terms of pH and the absence of bound metal. Each structure was superimposed onto the $^{\alpha}C$ trace of a minimized mean of the Spo0F ensemble using a program, Align, based on methods described Satow et al. (1986). These alignments gave the following rms deviations from the Spo0F backbone: 1.3 Å for the Spo0F Tyr13Ser mutant (114 $^{\alpha}C$ pairs), 2.0 Å for CheY (109 $^{\alpha}C$ pairs), 2.2 Å for NarL (115 $^{\alpha}C$ pairs), and 2.8 Å for NtrC (using model 1, 107 $^{\alpha}C$ pairs). A more meaningful approach was accomplished using the Kabsch and Sanders algorithm in PROCHECK to delineate secondary structure elements followed by the Align program to superimpose only the central sheets of the proteins onto Spo0F. The rms deviations for this alignment of 17 β-strand residues (N, $^{\alpha}C$, and C atoms) are 0.63 Å for the Spo0F Tyr13Ser mutant, 0.65 Å for CheY, 1.18 Å for NarL, and 1.06 Å for NtrC. Rms deviations on a residue by residue basis are plotted in Figure 4. Interhelical angles were measured using the method of Chothia et al. (1981) incorporated into the program InsightII (MSI, San Diego) by J. Theaker (Genentech, Inc.). The interhelical angles for

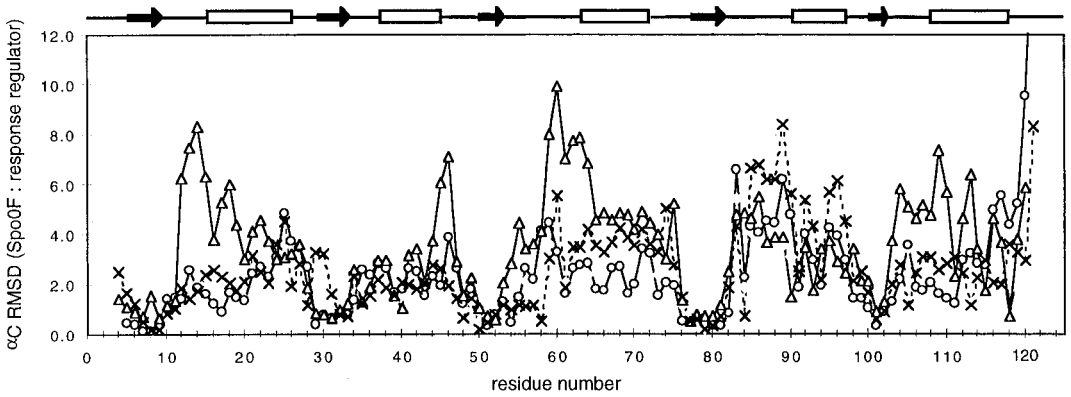

FIGURE 4: rms deviation between Spo0F and response regulator structures. The rms deviations between the αC traces of Spo0F and response regulators NarL (×), CheY (○), and NtrC (△) are plotted for each residue (Spo0F sequence numbering). The protocol used for aligning the structures is discussed in Experimental Procedures. The secondary structure elements of Spo0F are illustrated at the top as a reference; solid arrows indicate β-strands, and rectangles indicate α-helices.

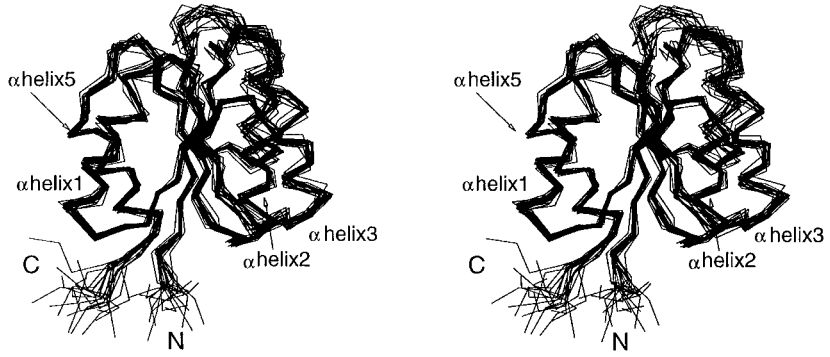

FIGURE 5: Superposition of 20 lowest-energy ⟨SA⟩ conformers of Spo0F. Stereoview of the αC backbone trace of Spo0F ensemble of structures. Figures 5, 7, and 9 were generated using INSIGHT II (MSI Technologies, Inc., San Diego).

each response regulator are reported in Table 3 of the Supporting Information.

RESULTS

Side Chain ^{13}C and ^{1}H Assignments. The complete ^{1}H, ^{15}N, and ^{13}C chemical shift assignments of Spo0F are tabulated in Table 1 of the Supporting Information. Backbone ^{1}H, ^{15}N, and ^{13}C assignments and secondary structure analysis were previously reported (Feher et al., 1995). The H(CCO)NH and C(CO)NH experiments were used to assign the remaining side chain ^{1}H and ^{13}C chemical shift values and confirm previous sequential assignments (see Experimental Procedures). These experiments were carried out using gradient methodology that allowed assignment of several amide protons previously unobserved because of fast exchange with solvent, primarily those residing in loop regions, e.g. residues Asp11−Tyr13. The use of ^{1}H, ^{15}N, and ^{13}C triple-resonance experiments also clarified the amide shifts for Asp11, Gln12, and Gly14 that were previously reported as Asp54, Met55, and Gly59, respectively (Feher et al., 1995). The side chain assignments also aided in resolving several amide protons that are directly overlapped, namely Met89 with Lys67 and Lys116 with Tyr118.

Structures. A superposition of the 20 lowest-energy structures of Spo0F is shown in Figure 5, and their statistics are given in Table 2. These structures have an overall rms deviation of 0.59 ± 0.06 Å for backbone atoms and 1.02 ± 0.06 Å for all heavy atoms (residues 5−81 and 91−120; Figure 6). All these structures have energies lower than 122 kcal mol^{-1}, no NOE violations greater than 0.22 Å, and no dihedral angle violations greater than 0.9°.

Table 2: Restraint Violation and Energy Statistics for Spo0F Structures

	ensemble	mean[a]
energy (kcal·mol^{-1})		
total	119.9 ± 3.03	113.0
bond lengths	4.38 ± 0.28	3.87
bond angles	101.8 ± 1.1	99.3
improper	8.76 ± 0.19	8.48
van der Waals	3.55 ± 1.14	1.30
restraint violation	1.14 ± 0.83	na
NOE violations		
no. >0.01 Å	72.9 ± 13.4	62
no. >0.1 Å	0.4 ± 0.6	0
maximum violation (Å)	0.22	0.06
dihedral angle violations		
no. >0.1°	5.6 ± 2.3	7
maximum (deg)	0.9	0.14
rms deviations from ideality		
bond lengths (Å)	0.002 ± 0.001	0.001
bond angles (deg)	0.424 ± 0.002	0.42
impropers (deg)	0.241 ± 0.003	0.235
rms deviations from experimental data		
NOE restraints (1504) (Å)	0.004 ± 0.001	0.001
H bonds (80) (Å)	0.002 ± 0.002	0.001
dihedral angle (239) (deg)	0.005 ± 0.002	0.022

[a] Values are calculated for the minimized mean of the 20 structure ensemble. na, not available.

Analysis of the ensemble with PROCHECK (Laskowski et al., 1993) indicates that 72.5 and 24.5% of the residues are in favorable or allowed regions of the Ramachandran diagram, respectively. No single residue is consistently in the generous or disallowed regions, and the vast majority of residues in such regions are in disordered parts of the ensemble. Thus, when the PROCHECK analysis is limited

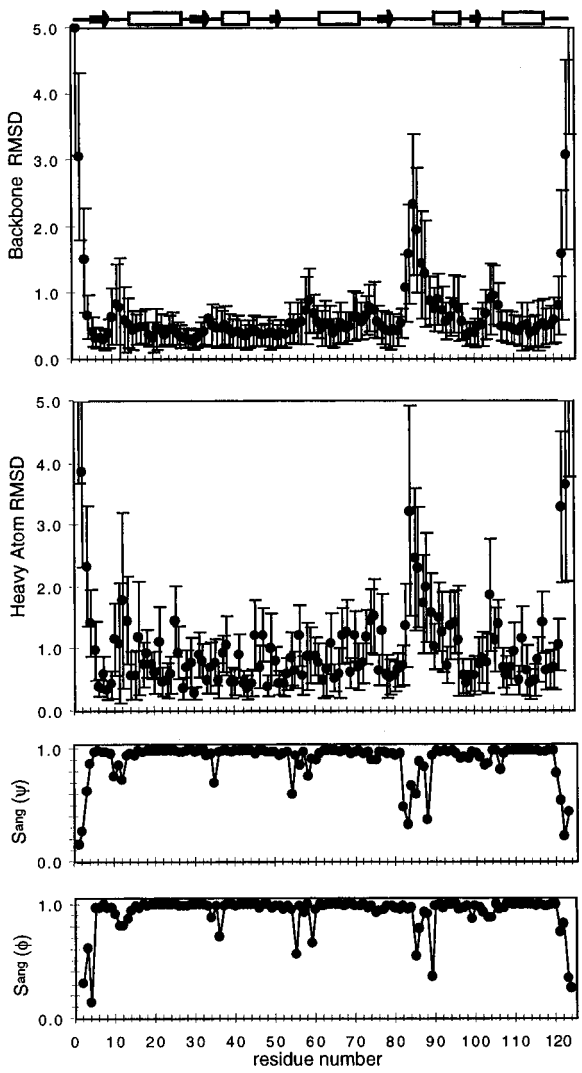

FIGURE 6: Rms deviations and dihedral angle order parameters for Spo0F structures. Backbone and heavy atom rms deviation values (angstroms) and S^{ang} (χ) and S^{ang} (ψ) dihedral angle order parameters (Hyberts, 1992) calculated for the 20 lowest-violation energy structures are plotted for each residue.

to residues for which S^{ang} (ϕ) and S^{ang} (ψ) are greater than 0.9, 86.5 and 13.4% of residues are in favorable and allowed regions, respectively (99.9% total).

The quality of the ensemble was also analyzed with respect to side chain orientation. Most of the well-ordered side chains [S^{ang} (χ_1) > 0.9] are within 30° of the classical staggered conformations: +60, −60, or 180°. However, some residues preceding and within α-helix 1 (Tyr13, Leu18, Asn20, Asn24, and Glu26) and the β4−α4 loop (Ile80, Tyr84, and Gln91) have well-defined χ_1 values more than 30° from the staggered values. As will be described in more detail below, other NMR parameters indicate that both of these regions exhibit molecular motions on a time scale of microseconds or longer. These motions may be responsible for time averaging of the NOE volumes. Thus, the derived NOE distance restraints cannot be satisfied by a single conformation, and the local geometry (χ_1) is perturbed. Despite the difficulties with NOE restraints in these isolated regions, most distance and dihedral angle restraints were sufficient to converge an ensemble of structures to a single conformation over 87% of the protein.

The global structure of Spo0F is an $(\alpha/\beta)_5$ fold (Figure 7) containing a central five-stranded parallel β-sheet surrounded

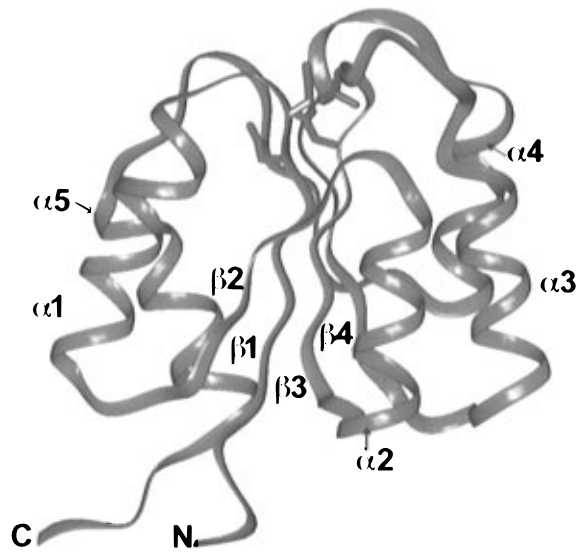

FIGURE 7: Ribbon diagram of the ⟨SA⟩ Spo0F structure. Spo0F has a $(\alpha/\beta)_5$ general fold with α-helices 2−4 on one side of the central parallel β-sheet and α-helices 1 and 5 on the other (β-strand 5 at the back of the molecule is not labeled). The side chain heavy atoms of the three aspartate residues comprising the phosphorylation site at the C termini of β-strand 1 (Asp10 and Asp11) and β-strand 3 (Asp54) are indicated in red, and Thr82 at the top of β-strand 4 is indicated in green.

by five α-helices. The termini of α-helices and β-strands were determined by the algorithm of Kabsch and Sanders (1983). The α-helices span residues Ile15−Glu26, Leu37−Lys45, Ile63−Ile72, Ile90−Gly97, and Ile108−Tyr118, and the β-strands span residues Lys5−Val9, Gln29−Ala33, Leu50−Leu53, Arg77−Met81, and Thr100−Phe102. These are generally the same as previously reported by analysis of primary NMR parameters (Feher et al., 1995).

The three central β-strands β1, β3, and β4, constitute the hydrophobic core of the protein. Nine hydrophobic residues define the packing of helices to this central core: Leu19 and Phe23 (α-helix 1), Ala39 and Val43 (α-helix 2), Ile65, Leu66, and Met69 (α-helix 3), and Ile111 and Val115 (α-helix 5). These residues are highly conserved throughout response regulators and were predicted to be important in hydrophobic core packing interactions (>80%; Volz, 1993). α-Helix 4 has few packing contacts with the central core; its orientation is dependent on van der Waals interactions and hydrogen bonds with α-helix 3 and β-strand 5 (Met89, Ile90, Lys94, and Leu96).

Genetic and biochemical analyses have shown that residues important in phosphorylation and activation of response regulators are Asp10, Asp11, Asp54, Thr82, and Lys104 (Saunders et al., 1989; Bourret et al., 1990; Volz, 1993). The side chains of these residues, with the exception of Lys104, are brought into close proximity by their positions at the C-terminal ends of β-strands 1, 3, and 4. The aspartyl pocket created by residues 10, 11, and 54 is consistent with the involvement of these residues in phosphorylation and magnesium binding. The $^{\gamma}$OH of Thr82 is directed at the aspartyl pocket (Thr82 $^{\gamma}$OH 4.9 ± 0.6 Å from Asp54 $^{\delta 1}$O), close enough to participate either in phosphorylation or, as recently suggested, in autophosphatase activity (Zhu et al., 1997). Primary NMR data suggest there is heterogeneity in the position of the Thr82 side chain; the weak signals in both the ^{13}C−^{15}N and ^{13}C−^{13}C J coupling experiments are consistent with averaging of the χ_1 angle rotamer, and NOEs

to the β- and γ-protons cannot be simultaneously satisfied. Sources of this heterogeneity are discussed later. The exact position of the Lys104 side chain is not well-determined because NOEs are not observed to side chain nuclei beyond the C^{β}.

Intramolecular Dynamics. High rms deviations for isolated regions of an ensemble of structures reflect underdetermination due to the lack of distance and dihedral angle restraints. Residues may have few observable NOEs and/or little rotamer averaging because they are located in regions with backbone flexibility. Individual residues of Spo0F that have backbone rmsd values greater than the mean rmsd from the mean structure include the N and C termini (Met1−Glu4 and Leu121−Asn124), the β1−α1 loop (Asp10−Gln12), the β3−α3 loop (Pro58−Gly59), the α3−β4 loop (Glu74−Asn75), the β4−α4 loop (Ala83−Glu92), part of α-helix 4 (Glu95−Leu96), and the β5−α5 loop (Lys104−Phe106). Most, but not all, of these residues have low values of S^{ang} (ϕ) and S^{ang} (ψ). ^{15}N amide relaxation parameters were analyzed to provide an independent measure of backbone dynamics. Figure 3 illustrates the measured T_1 and T_2 relaxation rates and T_1/T_2 ratios. The uniformity in the T_1 relaxation rate constants indicates that the protein is tumbling isotropically. Average values for T_1, T_2, and NOEs are 450 ± 30 ms, 100 ± 10 ms, and 0.78 ± 0.1, respectively. An overall correlation time of 7.0 ± 0.5 ns was calculated for Spo0F, a value consistent with isotropic tumbling of a monomeric protein this size. These parameters were analyzed using an adaptation of the Lipari−Szabo formalism as described by Kay et al. (1989) and Zhou et al. (1996) to provide order parameters (S^2), values reported in Table 2 of the Supporting Information. The order parameters suggest that there is a high degree of rigidity in regular secondary structure elements ($S^2 = 0.90 \pm 0.05$) for helices 2, 3, and 5 and β-strands 1−4 and correlate well with regions of low rms deviation. Of the residues with high rms deviations, most have low order parameters, indicating the lack of observable NOEs arises from dynamics inherent to the protein in these regions. These residues are located in loops or the N and C termini. This relationship between secondary structure and order parameters is commonly observed in proteins (Palmer, 1993).

Several regions of the protein have relaxation parameters that could not be fitted to the basic Lipari−Szabo model: Asp11−Gly14, Arg16−Gly27 (α-helix 1), Gly59, Lys70, Thr82, Gly85, Lys94, Thr100, and Phe102. The inability of the Lipari−Szabo model to adequately describe the relaxation behavior of these residues suggests there are additional chemical or conformational exchange contributions to the nitrogen relaxation rates on the microsecond to millisecond time scale which are not accounted for in the model used. These residues (with the exception of Asp11, Gln12, Gly59, and Gly85) correlate with the residues which have low rms deviations (0.46 ± 0.09). Further analysis of the dynamics data using methodologies which include exchange contributions (Mandel et al., 1995) will be reported elsewhere. Residues Asp11, Gln12, Gly59, and Gly85 appear to have significant solvent exchange as judged by comparison of HSQC spectra collected with gradient solvent suppression versus spectra collected with presaturation techniques.

Two Conformations in the C-Terminal β-Strand. Spo0F at pH 6.85 has two conformations in the C-terminal region

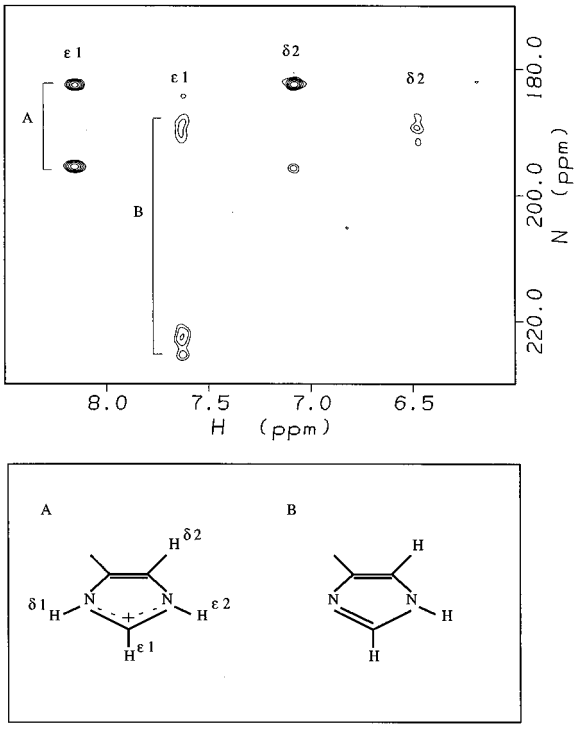

FIGURE 8: ^{1}H, ^{15}N HMBC of Spo0F illustrating the histidine 101 ring protonation state at pH 6.8. The top panel shows the HMBC spectrum collected on a 2 mM ^{15}N-, ^{13}C-labeled Spo0F sample. Two sets of $H^{\epsilon 1}$ and $H^{\delta 2}$ resonances are observed for the single histidine ring at pH 6.8. The proton resonances are correlated with nitrogen chemical shift patterns characteristic of two ionization states for the histidine ring (lower panel), the protonated form (A), and the neutral form (B) (Pelton et al., 1993).

of the protein. Two sets of side chain resonance assignments are observed for residues His101 and Phe102 from analysis of the C(CO)NH and H(CCO)NH spectra and the CT-HSQC spectrum of the aromatic region (Table 1 in the Supporting Information). Previous studies had indicated that conformational averaging was present in the β-strand 5 region through observation of intermediate $^3J_{HN\alpha}$ coupling constants, weaker than expected cross-strand NOEs, and relatively little protection from amide hydrogen exchange (Feher et al., 1995). In addition, amide proton line widths for Thr82, His101, Phe102, Ala103, and Lys104 resonances are broader than those observed for other resonances in ^{1}H-, ^{15}N-HSQC spectra. The spin systems corresponding to His101 and Phe102 within the same conformational state of Spo0F could be deduced from NOEs observed between these two side chains in the ^{15}N-, ^{13}C-edited NOESY-HSQC spectrum.

The multiple conformations appear to be pH-dependent. An HMBC experiment correlates the two sets of ring proton assignments for His101 to the two protonation states of the histidine at this pH (Figure 8; Pelton et al., 1993). The population of these two conformers at pH 6.85 is approximately 3:1 (neutral His:charged His) on the basis of relative peak intensities in the C(CO)NH and H(CCO)NH spectra. Only one set of histidine and phenylalanine resonances are observed at pHs higher than pH 7.3 corresponding to neutral His101. Conversely, at pH 5.9, only signals for the protonated histidine are observed (data not shown). Also, ^{1}H-, ^{15}N-HSQC amide proton line widths for Thr82, Phe102, Ala103, and Lys104 sharpen, and the resonance from His101 becomes more intense as pH is

increased, suggesting the conformational averaging observed in β-strand 5 region shifts to one conformer at higher pH.

NOEs specific to each conformational state were identified in the ^{15}N-, ^{13}C-edited NOESY-HSQC spectrum and two-dimensional NOESY spectra acquired with the [$\delta_{1,2}$,$\epsilon_{1,2}$-$^2H_4$]-Tyr and [$\delta_{1,2}$,$\epsilon_{1,2}$,ζ-$^2H_5$]Phe labeled samples in D_2O. The two-dimensional NOESYs generated 31 assignable distance restraints to His101 and Phe102 ring protons for the neutral conformer. Few NOEs to the alternate set of ring assignments are observable because of spectral overlap in the case of Phe102 or the lower population of this form. Structures were calculated using only those NOEs assigned to the neutral conformer. Several residues, Thr82, Ile80, and Ser93, in close proximity to His101 and/or Phe102 consistently had NOE violations suggestive of hydrogen positions which could not be simultaneously satisfied by a single conformation; these NOEs were omitted. These residues do not have conformational differences large enough to provide unique chemical shifts in each conformer, or the chemical shift difference is far less than the frequency of the exchange between the conformers.

There is additional conformational averaging in the neutral form itself which is manifested in the broadened resonances in the ^{15}N dimension of His101 in the HMBC (Figure 8); the structural consequences of this are unknown.

Comparison of Apo-Spo0F and Ca^{2+}-Bound Spo0F Tyr13Ser Mutant Structures. The crystal structure for the Ca^{2+}-bound Spo0F Tyr13Ser mutant has recently been reported (Madusudan et al., 1996). The mutant has an overall fold similar to the wild type structure reported here, with a backbone rms deviation of 0.97 Å for 115 $^{\alpha}$C pairs. Residues with the highest rms deviations are Gly14, Lys56, the γ-loop (Pro58−Glu64), the α3−β4 loop, the β4−α4 loop, and Pro105. High backbone deviations at Gly14 and Lys56 are not surprising because Gly14 is adjacent to the mutation site and the amide of Lys56 is involved in coordination of Ca^{2+} at the mutant active site.

Comparison of changes at the site of mutation reveals minor structural differences. In the mutant structure, the backbone at position 13 adopts a helical conformation and hydrogen bonds of Ile17 NH···OC Ser13 and Arg16 NH···OC Gln12 provide one additional helical turn relative to the wild type structure. Additional differences are observed in the χ_1 angles for the residues at position 13 ($-165.5 \pm 20°$ for Tyr13 and $-26.2°$ for Ser13). This results in significant change for side chain orientation at position 13; the Tyr13 ring packs against α-helix 1 over Arg16 and Ile17 in the wild type structure, and the Ser13 is solvent-exposed directly over the hydrophobic patch at the α1−α5 interface in the mutant. How these structural differences and the significant change in residue 13 hydrophobicity result in the inability for the Rap phosphatases to bind Spo0F and/or interfere in the dephosphorylation mechanism is unknown.

The other regions with large rms deviations between wild type and the mutant structure are located in loops that demonstrate high rms deviations within the wild type ensemble of structures and may be related to the internal dynamics discussed above. The mutant structure was solved under low-pH crystal conditions, conditions where the His101 imidazole ring is protonated (pH 4.5). The imidazole ring is only partially buried under the β4−α4 loop in the mutant structure. The His101 χ_1 angles are -166.9 ± 16.7 and 100.4° for the wild type and mutant, respectively, which results in a ring orientation with the $N^{\epsilon 2}$ atom solvent-exposed in the mutant as opposed to buried with a hydrogen bond to the amide of Thr82 in the wild type structure. The ensemble of wild type structures is not consistent with the His101 position observed for the mutant structure.

Comparison of Spo0F to Other Response Regulator Structures. Comparisons of the *B. subtilis* Spo0F structure to response regulators *E. coli* CheY, *S. typhimurium* NtrC, and *E. coli* NarL show they all have similar general folds; the rms deviations in the backbone of each with respect to *B. subtilis* Spo0F are 2.0, 2.8, and 2.2 Å, respectively. The structures have little deviation in the β-sheets ($\leq$1.0 Å deviation, Figure 4). However, significant differences are observed when the comparison includes α-helices. The rms deviations arise from subtle differences in the helix length, register, and helix axis angle. There is not a consistent correlation in the helical differences between response regulators. For example, α-helices 4 and 5 differ most between CheY and Spo0F, but comparisons of NarL and Spo0F show α-helices 3 and 4 differ most. Previous comparisons of structures in CheY have noted the large helix angle between α-helix 5 and α-helix 1 in CheY but not in other response regulators (Madusudan et al., 1996; Baikalov et al., 1996). Pairwise comparisons of the helices within each structure reveal that the relative helix angle stays about constant for α-helices 2 and 3, $15 \pm 6°$. Using these helices as a reference, comparisons of helix angles within and between response regulators suggest no consistent correlation of helix angles. For example, the angles between α-helix 2 and α-helix 4 can vary from 9° for Spo0F to 60° for NarL. The helix angle differences between Spo0F and α-helix 1 in NtrC, α-helix 4 in NarL, and α-helices 1, 4, and 5 in CheY are responsible for the high rms deviations observed in the backbone regions (Figure 4). Previously, comparisons based on primary sequence alignments and the CheY structure suggested conservation of secondary structure and global fold throughout response regulators (Volz, 1993); the comparison made here suggests there are sufficient differences in the surface architecture of the α-helices to provide specificity for each cognate kinase and target.

DISCUSSION

The analysis of solution structure and backbone dynamics of *B. subtilis* Spo0F reported here provides insights into several areas of interest concerning bacterial response regulators. The following discussion describes structural and dynamic factors that may influence response regulator magnesium affinity, phosphorylation lifetimes, and protein−protein interactions.

Factors Important in Phosphorylation Stability. The sequence and structural conservation of the active site residues required for phosphorylation and magnesium ion coordination throughout the family of response regulators suggests conservation of the phosphoryl-transfer mechanism. For example, crystallographic studies of Mg^{2+}-bound CheY and the Ca^{2+}-bound Spo0F Tyr13Ser mutant reveal that the same conserved aspartate residues are responsible for divalent cation coordination, namely Asp11 and Asp54 (13 and 57 in CheY), and the carbonyl of Lys56 (Asn59 in CheY; Stock et al., 1993; Madusudan et al., 1996). NMR studies of magnesium binding to wild type Spo0F support the observation that the ion is coordinated in a similar manner (Feher

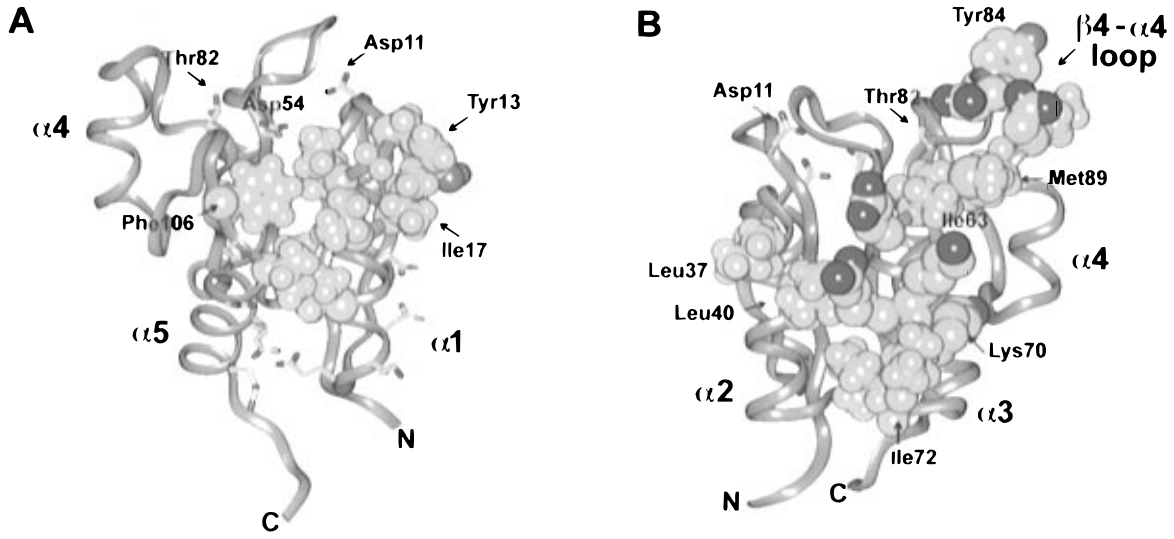

FIGURE 9: Clusters of hydrophobic surfaces on Spo0F. Ribbon representations of the ⟨SA⟩ Spo0F structure (green ribbon) are shown with residues contributing to the two surface-exposed hydrophobic clusters as CPK atoms (hydrophobic atoms in yellow). Panel A shows the α-helix 5−α-helix 1 interface (−110° *y*-axis rotation relative to Figure 7) where residues Tyr13, Gly14, Ile15, Ile17, Leu18, Val22, Phe106, and Ile108 make up a hydrophobic region close to the active site. Charged residues (red) and polar residues (blue) are also indicated. Panel B shows the surface of α-helices 2−4, extending to the *β*4−α4 loop (∼90° *y*-axis rotation relative to Figure 7) where residues Leu37, Leu40, Ile63, Val71, Ile72, and Met89 and the aliphatic atoms of Glu64, Lys67, Arg68, and Lys70 contribute to this hydrophobic surface.

et al., 1995). Despite the structural conservation of the chelating side chains, a wide range of magnesium binding affinities and phosphorylation lifetimes are observed for these proteins (Lukat et al., 1990; Zapf et al., 1996; Feher et al., 1995). The magnesium affinities for *E. coli* CheY and *B. subtilis* Spo0F are 0.5 and 20 mM and their phosphorylation half-lives 20 s and 12 h, respectively. Comparison of active site structure and dynamics for these proteins provides possible explanations for these differences.

Madusudan et al. (1996) made structural comparisons of the nonconserved residues near aspartyl pockets for Spo0F and CheY, noting differences which reduce the hydrophobic content of residues surrounding this pocket relative to those observed in CheY. This conclusion is supported by previously reported hydrogen exchange studies for Spo0F, revealing high solvent accessibility to these residues (Feher et al., 1995). The backbone dynamics reported here for Spo0F suggest that the loops comprising the active site have a high propensity for chemical exchange and are highly flexible. A glycine at position 14 allows this loop more conformational flexibility than observed in other response regulators which commonly have a hydrophobic residue at this position. Taken together, these observations suggest that magnesium may not form a tight coordination complex with Spo0F because of the solvation and inherent flexibility in the residues required for coordination.

The metal ion is thought to be important in stabilization of the transition state for both the phosphoryl-transfer and hydrolysis reactions (Stock et al., 1993; Hershlag & Jencks, 1990). Therefore, the lower Mg^{2+} binding affinity of Spo0F is likely to decrease the ability of the protein to stabilize these transition states. The lowered capacity to stabilize the transition state for phosphoryl transfer during autophosphorylation reactions with chemical phosphodonors may explain the apparent selectivity Spo0F has for the more easily catalyzed transfer from phosphoramidates versus acyl phosphate compounds (Zapf et al., 1995). This selectivity would prevent Spo0F from becoming activated by metabolic signaling molecules such as acetyl phosphate *in vivo*, a possibility that has been suggested for other response regulators (McCleary et al., 1993). Finally, the lower capacity to stabilize the transition state for the hydrolysis reaction is consistent with the longer phosphorylation lifetime of Spo0F relative to those of other response regulators that have higher magnesium affinities.

Relative magnesium affinities may not entirely explain the comparative phosphorylation lifetimes observed for response regulators. It has been suggested that the proximity of a basic lysine side chain to Asp54 may also enhance the relative stability of phospho-Spo0F compared to that of phospho-CheY through stabilization of the phosphorylated ground state (Madusudan et al., 1996). The proximity of Lys56 to Asp54 (6.4 ± 1.2 and 6.7 ± 1.1 Å from Lys56 $^{\zeta}NH_3$ to Asp54 $O^{\delta 1}$ and $O^{\delta 2}$, respectively) is also observed in the wild type solution structure reported here. Lys56 may make favorable electrostatic interactions with one of the phosphoryl oxygens when the acyl phosphate forms at Asp54. Consistent with this hypothesis, substitution of Lys56 with asparagine in Spo0F significantly increases the auto-dephosphorylation rate (J. W. Zapf, unpublished results).

Thus, the relative phosphorylation lifetimes for response regulators may be controlled by the nature of nonconserved residues at the site of phosphorylation. Through modification of these residues, factors important for phosphoryl transfer and acyl phosphate stability can be altered, e.g. solvent accessibility, backbone dynamics, magnesium affinity, and potential salt bridge interactions. In this way, the phosphorylation lifetimes of the response regulators may be customized to fit the needs of their signaling pathway.

Potential Protein−Protein Interaction Surfaces. Spo0F must provide protein surfaces for interaction with three types of proteins: kinases, phosphatases, and a phosphotransferase, Spo0B. Analysis of hydrophobic and electrostatic surfaces on Spo0F combined with recent genetic evidence suggests two potential regions for protein−protein interactions.

Figure 9 illustrates the exposed hydrophobic and electrostatic surfaces on Spo0F. There are two patches of exposed hydrophobic residues: (1) the surface at the N-terminal

interface of α-helix 1 and α-helix 5 (residues Gly14, Ile15, Ile17, Leu18, Val22, Pro105, Phe106, and Ile108) and (2) the surface of α-helix 2, α-helix 3, and the β4−α4 loop (residues Leu37, Leu40, Ile63, Lys67, Arg68, Val71, Ile72, Leu87, and Met89). This second region describes a slightly larger area of hydrophobic surface than previously noted for the crystal structure Spo0F Tyr13Ser mutant (Madusudan et al., 1996) by the inclusion of residues Ile63, Lys67, Arg68, Leu87, and Met89, extending the surface to the top of β4−α4 loop. Both of these regions are surrounded by charged residues and are likely to be important for stabilizing protein−protein interactions.

The hydrophobic patch at the α-helix 1 and α-helix 5 interface may be important in response regulator−phosphatase interactions. Inspection of the loop region at the top of α-helix 1 (Figure 9A) shows Tyr13 is clearly exposed to solvent and, along with Ile17 and Leu18, is located in one of the two hydrophobic regions on the protein surface mentioned above. The Tyr13Ser mutation abrogates acyl phosphate hydrolysis by RapA (Perego & Hoch, 1994). Mutations in CheY (Asn23Asp and Lys26Glu) which decrease the CheZ phosphatase activity (Sanna et al., 1995) are located on α-helix 1 near a similar hydrophobic region of CheY. From these studies alone, it is unclear whether the phosphatase resistance is derived from the alteration of potential protein−protein contacts or from changing residues important in an allosteric response to the phosphatase (Sanna et al., 1995).

Additionally, alanine scanning of Spo0F for non-active site residues which display a sporulation deficient phenotype identified several residues located in the β4−α4 loop region, the N-terminal end of α-helix 4 and the N-terminal interface of α-helix 5 and α-helix 1 may be important for kinase and Spo0B interactions (Y.-L. Tzeng and J. Hoch, personal communication). All these sites are in proximity to the hydrophobic regions described.

Spo0F Surfaces with a Propensity for Multiple Conformers. Because both unphosphorylated and phosphorylated Spo0F participate in protein−protein interactions with different proteins in the pathway, there is likely to be some surface structural or dynamic manifestation of alternate conformers that allows recognition of a particular Spo0F phosphorylation state by the appropriate protein. The results from analysis of Spo0F backbone dynamics define regions of the protein which have a propensity for multiple conformers. One set of residues (Asp11−Gly14 and Gly59) comprise the regions in proximity to the phosphorylation site. Interestingly, two other regions, α-helix 1 and the β4−α4 loop and α-helix 4 and β-strand 5, overlap with the surfaces defined above as potential sites for protein−protein interaction. It is probable that the conformations of both of these regions are closely tied to the conformational state of the active site; α-helix 1 (Asn20 and Val22) and C-terminal (Thr82, Phe102, and Lys122) amide resonances are sensitive to magnesium binding at the active site (Feher et al., 1995). Also, amide resonances sensitive to phosphorylation of CheY are found in α-helix 1, the β4−α4 loop, α-helix 4, β-strand 5, and α-helix 5 (Lowry et al., 1994).

The chemical/conformational exchange observed for residues Lys70, Thr82, Gly85, Lys94, Thr100, and Phe102 are related to the slow exchange between the two His101 conformations observed in the β-strand 5 region. All of these residues can be structurally linked. The Thr82 amide proton is a hydrogen bond donor for $N^{\epsilon 2}$ on the His101 imidazole ring, and Thr100 and Phe102 are His101 neighbors; the amide hydrogen of Lys94 has a hydrogen bond to carbonyl of Ile90, and the Lys70 side chain amino group (on α-helix 3) has a hydrogen bond with the backbone carbonyl of Leu96 of α-helix 4. Gly85 is in the loop linking β4 and α-helix 4. In addition, there are hydrophobic packing interactions between α-helix 3, α-helix 4, and β-strand 5. The dynamics therefore suggest this region, the β4−α4 loop, the C terminus of α-helix 3, α-helix 4, and β-strand 5 behave in a concerted manner dependent upon the histidine conformation. The structural consequences of alternate histidine conformations are illustrated by comparison of the β4−α4 loop region of the wild type structure reported here and the crystal structure of the Spo0F Tyr13Ser mutant.

The functional significance of the multiple histidine conformations is unclear. Two conformations are observed for residue Tyr106 in the crystal structure of apo-CheY (Volz & Matsumura, 1991); the Tyr106 ring adopts either a buried or solvent-exposed position. This residue is homologous to the His101 of Spo0F; however, the structural perturbations in CheY do not extend to neighboring residues in β-strand 5, α-helix 4, and α-helix 3 as observed in Spo0F. Recent structural elucidation of several CheY mutations has suggested the position of the tyrosine ring correlates with the signaling state of the protein (Zhu et al., 1997). The His101Ala mutation in Spo0F results in a hypersporulation phenotype (Y.-L. Tzeng, unpublished results). Studies are underway to biochemically characterize this mutant. Thus, our observations of the conformational sensitivity of this region to pH may be a manifestation of this region's propensity for conformational change upon phosphorylation. The difficulty in determining the conformational differences between the two forms suggests that the putative conformational change for regions other than the β4−α4 loop may be very subtle.

ACKNOWLEDGMENT

The authors acknowledge Logan Donaldson, Doug Juers, and Hong-Jun Zhou for aid in data collection and analysis. Thanks to Yih-Ling Tzeng for useful discussions and comments on the manuscript and to Patricia Jennings at the University of California at San Diego for the use of the NMR facilities for part of this work.

SUPPORTING INFORMATION AVAILABLE

^{15}N, ^{13}C, and ^{1}H resonance assignments for Spo0F at pH 6.8 and 27 °C (Table 1), ^{15}N relaxation parameters and backbone order parameters for Spo0F (Table 2), and comparison of angles between α-helices for response regulator structures (Table 3) (13 pages). Ordering information is given on any current masthead page.

REFERENCES

Archer, S. J., Ikura, M., Torchia, D. A., & Bax, A. (1991) *J. Magn. Reson. 95*, 636−641.

Baikalov, I., Schroder, I., Kaczor-Grzesköwiak, M., Grzesköwiak, K., Gunsalus, R. P., & Dickerson, R. E. (1996) *Biochemistry 35*, 11053−11061.

Baker, E. N., & Hubbard, R. E. (1984) *Prog. Biophys. Mol. Biol. 44*, 97−179.

Barbato, G., Ikura, M., Kay, L. E., Pastor, R. W., & Bax, A. (1992) *Biochemistry 31*, 5269−5278.

Bax, A., & Summers, M. L. (1986) *J. Am. Chem. Soc. 108*, 2093−2094.
Bax, A., Clore, G. M., & Gronenborn, A. M. (1990a) *J. Magn. Reson. 88*, 425−431.
Bax, A., Clore, G. M., Driscoll, P. C., Gronenborn, A. M., Ikura, M., & Kay, L. E. (1990b) *J. Magn. Reson. 87*, 620−627.
Bellsolell, L., Prieto, J., Serrano, L., & Coll, M. (1994) *J. Mol. Biol. 238*, 489−495.
Bourret, R. B., Hess, J. F., & Simon, M. I. (1990) *Proc. Natl. Acad. Sci. U.S.A. 87*, 41−45.
Bourret, R. B., Drake, J. F., Chervitz, S. A., Simon, M. I., & Falke, J. J. (1993) *J. Biol. Chem. 268*, 13089−13096.
Brünger, A. T. (1992) *X-PLOR: A System for X-ray Crystallography and NMR*, Yale University Press, New Haven, CT.
Burbulys, D., Trach, K. A., & Hoch, J. A. (1991) *Cell 64*, 545−552.
Chothia, C., Levitt, M., & Richardson, D. (1981) *J. Mol. Biol. 145*, 215−250.
Driscoll, P. C., Gronenborn, A. M., & Clore, G. M. (1988) *FEBS Lett. 243*, 223−233.
Feher, V. A., Zapf, J. W., Hoch, J. A., Whiteley, J. M., Dahlquist, F. W., & Cavanagh, J. (1995) *Protein Sci. 4*, 1801−1814.
Ferrin, T. E., Huang, C. C., Jarvis, L. E., & Langridge, R. (1988) *J. Mol. Graphics 6*, 13−17.
Grzesiek, S. (1993b) *J. Biomol. NMR 3*, 487−493.
Grzesiek, S., Anglister, J., & Bax, A. (1993a) *J. Magn. Reson., Ser. B 101*, 114−119.
Herschlag, D., & Jencks, W. P. (1990) *J. Am. Chem. Soc. 112*, 1942−1950.
Hoch, J. A. (1993) *Annu. Rev. Microbiol. 47*, 441−465.
Hyberts, S. G., Goldberg, M. S., Havel, T. F., & Wagner, G. (1992) *Protein Sci. 1* (6), 736−759.
Ikura, M., Kay, L. E., & Bax, A. (1991a) *J. Biomol. NMR 1*, 299−304.
Ikura, M., Spera, S., Barbato, G., Kay, L. E., Krinks, M., & Bax, A. (1991b) *Biochemistry 30*, 9216−9228.
Jeener, J., Meier, B. H., Bachmann, P., & Ernst, R. R. (1979) *J. Chem. Phys. 71*, 4546−4553.
Kabsch, W., & Sander, C. (1983) *Biopolymers 22*, 2577−2637.
Kay, L. E., Torchia, D. A., & Bax, A. (1989) *Biochemistry 28*, 8972−8979.
Laskowski, R. A., MacArthur, M. W., Moss, D. S., & Thorton, J. M. (1993) *J. Appl. Crystallogr. 26*, 286−291.
Levitt, M. H., Freeman, R., & Frienkiel, T. (1982) *J. Magn. Reson. 47*, 328−330.
Lowry, D. F., Roth, A. F., Rupert, P. B., Dahlquist, F. W., Moy, F. J., Domaille, P. J., & Matsumura, P. (1994) *J. Biol. Chem. 269*, 26358−26362.
Lukat, G. S., Stock, A. M., & Stock, J. B. (1990) *Biochemistry 29*, 5436−5442.
Madusudan, Whiteley, J. M., Hoch, J. A., Zapf, J., Xuong, N. H., & Varughese, K. I. (1996) *Structure 4*, 679−690.
Mandel, A. M., Akke, M., & Palmer, A. G., III (1995) *J. Mol. Biol. 246*, 144−163.
Marion, D., Ikura, M., Tschudin, R., & Bax, A. (1989a) *J. Magn. Reson. 85*, 393−399.
Marion, D., Ikura, M., & Bax, A. (1989b) *J. Magn. Reson. 84*, 425−430.
McCleary, W. R., Stock, J. B., & Ninfa, A. J. (1993) *J. Bacteriol. 175*, 2793−2798.
Moy, F. J., Lowry, D. F., Matsumura, P., Dahlquist, F. W., Krywko, J. E., & Domaille, P. J. (1994) *Biochemistry 33*, 10731−10742.
Muchmore, D. C., McIntosh, L. P., Russell, C. B., Anderson, D. E., & Dahlquist, F. W. (1989) *Methods Enzymol. 177*, 44−73.
Neri, D., Szyperski, T., Otting, G., Senn, H., & Wuthrich, K. (1989) *Biochemistry 28*, 7510−7516.
Nilges, M. (1993) *Proteins 17*, 297−309.
Norwood, T. J., Boyd, J., Heritage, J. E., Soffe, N., & Campbell, I. D. (1990) *J. Magn. Reson. 87*, 488−501.
Palmer, A. G., III (1993) *Curr. Opin. Biotechnol. 4*, 385−391.
Parkinson, J. S., & Kofoid, E. C. (1992) *Annu. Rev. Genet. 26*, 71−112.
Pascal, S. M., Muhandiram, D. R., Yamazaki, T., Forman-Kay, J. D., & Kay, L. E. (1994) *J. Magn. Reson., Ser. B* 103, 197−201.
Pelton, J. G., Torchia, D. A., Meadow, N. D., & Roseman, S. (1993) *Protein Sci. 2*, 543−558.
Perego, M., & Hoch, J. A. (1996) *Proc. Natl. Acad. Sci. U.S.A. 93*, 1549−1553.
Perego, M., Cole, S. P., Burbulys, D., Trach, K., & Hoch, J. A. (1989) *J. Bacteriol. 171*, 6187−6196.
Perego, M., Hanstein, C., Welsh, K. M., Djavakhishvili, T., Glaser, P., & Hoch, J. A. (1994) *Cell 79*, 1047−1055.
Rance, M., Sørensen, O. W., Bodenhausen, G., Wagner, G., Ernst, R. R., & Wuthrich, K. (1983) *Biochem. Biophys. Res. Commun. 117*, 479−485.
Richarz, R., & Wüthrich, K. (1978) *Biopolymers 17*, 2133−2141.
Sanna, M. G., Swanson, R. V., Bourret, R. B., & Simon, M. I. (1995) *Mol. Microbiol. 15*, 1069−1079.
Santoro, J., & King, G. C. (1992) *J. Magn. Reson. 97*, 202−207.
Santoro, J., Bruix, M., Pascual, J., Lopez, E., Serrano, L., & Rico, M. (1995) *J. Mol. Biol. 247*, 717−725.
Satow, Y., Cohen, G. H., Padlan, E. A., & Davies, R. D. (1986) *J. Mol. Biol. 190*, 593−604.
Saunders, D. A., Gillece-Castro, B. L., Stock, A. M., Burlingame, A. L., & Koshland, D. E., Jr. (1989) *J. Biol. Chem. 264*, 21770−21777.
Senn, H., Werner, B., Messerle, B. A., Weber, C., Traber, R., & Wüthrich, K. (1989) *FEBS Lett. 249*, 113−118.
Shaka, A. J., Barker, P. B., & Freeman, R. (1985) *J. Magn. Reson. 64*, 547−552.
Shaka, A. J., Lee, C. J., & Pines, A. (1988) *J. Magn. Reson. 77*, 274−293.
Skelton, N. J., Aspiras, F., Ogez, J., & Schall, T. J. (1995) *Biochemistry 34*, 5329−5342.
States, D. J., Haberkorn, R. A., & Ruben, D. J. (1982) *J. Magn. Reson. 48*, 286−292.
Stock, A. M., Mottonen, J. B., Stock, J. B., & Schutt, C. E. (1989) *Nature 337*, 745−749.
Stock, A. M., Martinez-Hackert, E., Rasmussen, B. F., West, A. H., Stock, J. B., Ringe, D., & Petsko, G. A. (1993) *Biochemistry 32*, 13375−13380.
Stock, J., Surette, M. G., Levitt, M., & Park, P. (1995) *in Two-Component Signal Transduction* (Hoch, J. A., & Silhavy, T. J., Eds.) pp 25−51, ASM Press, Washington, DC.
Stock, J. B., Ninfa, A. J., & Stock, A. M. (1989) *Microbiol. Rev. 53*, 450−490.
Stone, M. J., Fairbrother, W. J., Palmer, A. G., Reizer, J., Saier, M. H., Jr., & Wright, P. E. (1992) *Biochemistry 31*, 4394−4406.
Trach, K. N., & Hoch, J. A. (1993) *Mol. Microbiol. 8*, 69−79.
Volkman, B. F., Nohaile, M. J., Amy, N. K., Kustu, S., & Wemmer, D. E. (1995) *Biochemistry 34*, 1413−1424.
Volz, K. (1993) *Biochemistry 32*, 11741−11753.
Volz, K., & Matsumura, P. (1991) *J. Biol. Chem. 266*, 15511−15519.
Vuister, G. W., & Bax, A. (1992) *J. Magn. Reson. 98*, 428−435.
Vuister, G. W., Wang, A. C., & Bax, A. (1993) *J. Am. Chem. Soc. 115*, 5334.
Wagner, G., Braun, W., Havel, T. F., Schaumann, T., Go, N., & Wüthrich, K. (1987) *J. Mol. Biol. 196*, 611−639.
Wishart, D. S., Sykes, B. D., & Richards, F. M. (1991) *J. Mol. Biol. 222*, 311−333.
Yamazaki, T., Forman-Kay, J. D., & Kay, L. E. (1993) *J. Am. Chem. Soc. 115*, 11054−11055.
Yip, P. (1990) *J. Magn. Reson. 90*, 382−383.
Zapf, J. W., Hoch, J. A., & Whiteley, J. M. (1996) *Biochemistry 35*, 2926−2933.
Zhou, H.-J., McEvoy, M. M., Lowry, D. F., Swanson, R. V., Simon, M. I., & Dahlquist, F. W. (1996) *Biochemistry 35*, 433−443.
Zhu, G., & Bax, A. (1992) *J. Magn. Reson. 100*, 202−207.
Zhu, X., Rebello, J., Matsumura, P., & Volz, K. (1997) *J. Biol. Chem. 272*, 5000−5006.

BI970816L